

A Calibration Procedure for a Bone Loading System

Sylvana García-Rodríguez

Department of Mechanical Engineering,
University of Wisconsin—Madison,
1513 University Avenue,
Madison, WI 53706-1572
e-mail: garcia1@wisc.edu

Everett L. Smith

Department of Population Health Sciences,
University of Wisconsin—Madison,
1300 University Avenue, Room 1097,
Madison, WI 53706
e-mail: elsmith1@facstaff.wisc.edu

Heidi-Lynn Ploeg

Department of Mechanical Engineering,
University of Wisconsin—Madison,
1513 University Avenue,
Madison, WI 53706-1572
e-mail: ploeg@engr.wisc.edu

Trabecular bone tissue is a three-dimensional structure that is difficult to duplicate with in vitro cell cultures or animal models. In an attempt to better understand the underlying mechanisms of tissue response to load, a system to load isolated bone preparations was developed. This ex vivo bone culture and loading system, given the name of ZETOS, compressively loads trabecular bone (10 mm diameter, 5.0 mm height) to evaluate its morphological and physiological responses while keeping cells viable. Compliance of the system may change with time, thus requiring recalibration. The purpose of this research was to develop and validate a recalibration protocol for the ZETOS system. Ten reference bodies (RBs) were designed and machined out of aluminum 7075-T6, with a structural rigidity range representative of trabecular bone (0.628–28.3 N/μm, or apparent elastic modulus of 40 MPa–1.80 GPa). Finite element analysis (FEA) was used to calculate the rigidity of each RB and was validated with physical testing in a universal testing machine. Results from FEA were then used to calibrate the system and relate force, piezoelectric actuator expansion, and specimen compressive deformation through a surface generated by spline interpolation, thus creating a calibration table. Calibration of ZETOS was verified by testing the RBs as well as three custom-made, metal springs and comparing measured rigidity to that calculated by FEA. Mean percent difference of FEA results with respect to those from physical testing was 3.28%. The mean percent difference of RB rigidity found with ZETOS with respect to rigidity found with FEA was 1.12% and for the metal springs, the mean percent difference was 1.74%. The calibration procedure for the ZETOS bone loading system has been successfully applied and verified. The use of RBs and FEA allows users to easily and periodically evaluate and recalibrate the system. Accuracy in studies of human bone mechanotransduction in a controlled environment can therefore be achieved. The recalibration procedure is relevant for other ZETOS users and may serve as the basis for calibration of other testing systems for small specimens of compliant materials. [DOI: 10.1115/1.2889059]

Keywords: trabecular bone, calibration, rigidity, finite element analysis

1 Introduction

Osteoporosis is a major health concern in the aging population, manifested by decreased osteoblastic activity, increased calcium loss, and low bone mineral density, resulting in diminished skeletal integrity and increased fracture risk. The greatest risk of fracture is in trabecular regions of the spine, hip, and wrist resulting in more than 1.5×10^6 fractures per year [1]. Vanness and Tosteson [2] estimated the total cost of osteoporosis in the United States, including medical care cost, research, and development, to be 34 billion in 2004 and projected to be 41.4 billion in 2025. While the resulting loss in bone strength and skeletal architecture in trabecular bone are clearly defined, the underlying mechanism is difficult to measure and determine. Bone cells, especially osteocytes, reside in a three-dimensional (3D) lattice that is not easily duplicated with in vitro cell culture studies. In animal models, due to the inaccessibility and nature of the mineralized tissue, physiological and morphological cellular responses are difficult to measure. In order to better investigate trabecular responses to both biochemical and mechanical stimuli, Jones et al. have developed an isolated bone preparation and loading system [3], in which trabecular bone may be maintained viable for up to 49 days [4–6]. This system, referred to as ZETOS, is an ex vivo culture and loading system designed to evaluate structural and cellular response of trabecular bone cylinders, 5.0 mm in height and 10 mm in diameter.

In the ZETOS loading system (Fig. 1), the bone cylinders are

axially compressed with a piezoelectric actuator (PZA) (Model P-239.30, Physik Instrumente, Karlsruhe, Germany), which expands with input voltage. Strain gages on the PZA measure its expansion; a load cell (Type 9011A, Kistler, Winterthur, Switzerland) measures the applied force. The strain gages are mounted in a Wheatstone bridge arrangement for temperature compensation. Due to the inherent compliance of the loading system, force and PZA expansion measurements are related through a calibration table to determine the compressive deformation of the specimen. ZETOS loading systems are currently used in several laboratories worldwide. They were calibrated when fabricated [3]; however, after multiple use cycles, the system's compliance, like any other mechanical system, will change. It is therefore necessary to have an uncomplicated method to calibrate the system at regular intervals to ensure accuracy. The purpose of the current study was to develop and validate a calibration protocol for the ZETOS bone loading system.

The elastic modulus of an isotropic, homogeneous material is the constant of proportionality between stress and strain within the elastic region. However, bone is heterogeneous, viscoelastic, and anisotropic. In trabecular bone, the anisotropy of the mechanical properties is mainly due to the structural arrangement of the trabeculae and not due to the "material" composition of the bone [7–9]. Therefore, it would not be appropriate to say that bone has a certain elastic modulus, but an *apparent* elastic modulus, determined from the bulk geometric measurements. This paper will refer to the term *rigidity*, which is "the load required to deform (a structure) a given amount" [8]. A structure's rigidity is the result of its geometry, including the size, as well as its mechanical properties. This paper will use the term *standard bone specimen* to

Manuscript received June 27, 2007; final manuscript received February 5, 2008; published online March 11, 2008. Review conducted by Vijay Goel.

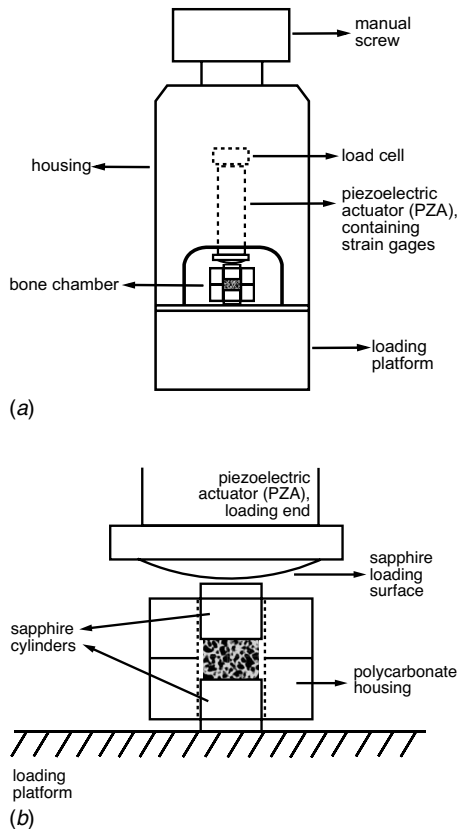


Fig. 1 (a) Schematic showing the ZETOS loading unit. The load cell, PZA, and bone chamber are arranged in series within the system. **(b)** A closer look at the bone chamber, where the trabecular bone sample is placed between two sapphire cylinders. The loading end of the PZA is comprised of a convex sapphire surface to account for nonparallel surfaces most likely present in the cylindrical bone sample.

refer to a trabecular bone cylinder of 10 mm diameter and 5.0 mm height. The rigidity of the standard bone specimen can be represented with any other structure having the appropriate combination of mechanical properties and geometry. For calibration purposes, a reference body (RB), with stable mechanical properties and known rigidity, was used to represent the rigidity of a standard bone specimen. Several RBs were required to cover a range of rigidity to accommodate the system's nonlinear compliance response to load and the variability of trabecular bone mechanical properties.

2 Methods

2.1 Reference Body Design and Development. Using finite element analysis (FEA), ten metal RBs (Fig. 2) were designed to have a rigidity range equivalent to that of standard bone specimens (0.628–28.3 N/ μm , or apparent elastic modulus of 40 MPa–1.80 GPa) [10]. They were labeled from 1 to 10 (RB1–RB10), from the least to the most stiff. Rigidity, K , is defined as

$$K = \frac{F}{\delta} \quad (1)$$

where F is force and δ is deformation.

The RBs were made of aluminum 7075-T6 for its machinability, corrosion resistance, and elastic modulus, as well as its non-viscoelastic behavior. Rigidity variation was achieved through geometric changes, focusing on diaphragm thickness and radius. The diaphragm deflects downward under compression applied through a solid piston, referred to as the RB piston (Fig. 2). For

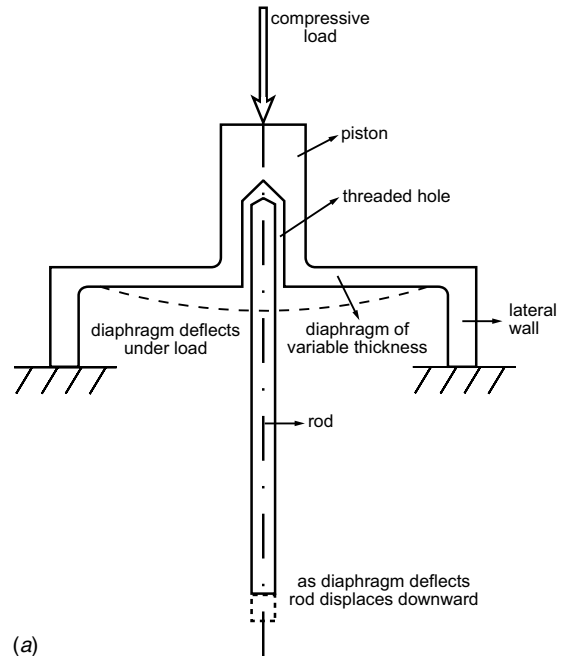


Fig. 2 (a) Schematic of a section view of a reference body (RB) and the stainless steel rod (not to scale). As the piston undergoes compressive load, the diaphragm deflects causing the downward displacement of the rod. **(b)** Geometry of a RB in three-dimensional representation, sectioned through the middle (rod not shown).

small diaphragm thickness-to-radius ratio, the rigidity (F/δ_{max} , or load/diaphragm deflection) is related to diaphragm thickness (h), radius (r), and elastic modulus (E) with

$$\delta_{\text{max}} = k_1 \frac{Fr^2}{Eh^3} \quad (2)$$

The coefficient k_1 is a function of the ratio of the diaphragm and the piston radii [11].

The RB design had to comply with geometric constraints of the loading unit, which did not permit direct measurement of diaphragm deflection. Therefore, a cylindrical stainless steel rod (5.0 mm diameter, 109.5 mm length) was threaded in the central, bottom surface of the piston. The downward movement of the rod corresponded to diaphragm deflection.

2.2 ZETOS Piezoelectric Actuator Expansion and Load. A fiber optic distance sensor (RC12-C1R, Philtec, Inc., Annapolis, MD) was used to calibrate the PZA expansion. The ZETOS load-

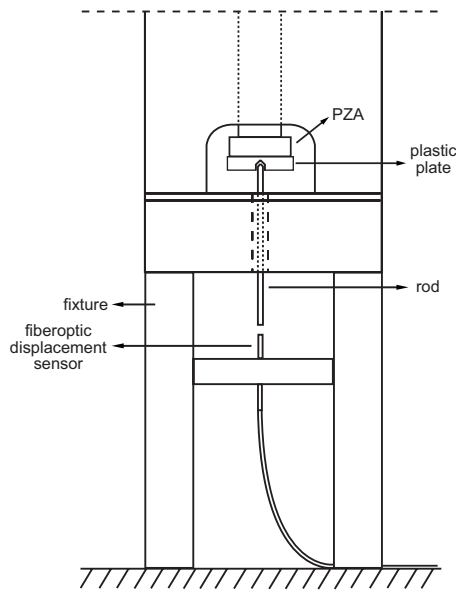


Fig. 3 Experimental setup for calibration of the strain gage by measuring the PZA expansion. Voltage is applied to the PZA causing its expansion. The lack of load allows the measurement of rod displacement obtained with the fiber optic sensor to directly represent PZA expansion without system compliance effects.

ing unit was placed on an aluminum fixture that held the sensor in place directly underneath the rod, which was attached to the end of the PZA and protruded through a hole in the base of the loading system (Fig. 3). All measurements were performed at room temperature. Maximum voltage (1000 V) was applied to the PZA causing its full expansion; due to the absence of a specimen, the actuator was free to expand without resistance. The output voltage of the sensor was related to the distance between its tip and the rod's surface through a calibration curve supplied by the manufacturer. Its operating range was from 0.000 mm to 0.510 mm (0–5 V) with precision of $0.3 \mu\text{m}$ and sensitivity of $43.1 \mu\text{m}/\text{V}$. The sensor's accuracy was verified using a three-axis MicroBlock™ flexure stage (Model MBT616, Thorlabs, Inc., Newton, NJ), with resolution of $0.02 \mu\text{m}$, and a coordinate measuring machine (CMM) (Zeiss Spectrum, Carl Zeiss, Inc., Thornwood, NY) with a resolution of $2 \mu\text{m}$. The displacement of the rod was calculated as the change in distance from the initial position. The rod displacement measured by the fiber optic sensor corresponded to PZA expansion. Its signal was acquired and conditioned using a data acquisition system (DAQ Card 6024E, National Instruments, Austin, TX) and LabVIEW version 7.1 (National Instruments, Austin, TX).

To relate the loading system's force and PZA expansion, the ten RBs were tested with ZETOS at room temperature in random order, ten times each, with a preload of 10 N. To avoid indentation of the aluminum RB piston (Fig. 2), a sapphire cylinder (10 mm diameter, 10 mm height) was placed between the RB and the PZA, whose loading end is made of a convex, sapphire crystal (65.2 mm radius). The RBs were loaded within the limits of ZETOS (maximum force, PZA expansion, or RB compression of 1500 N, $70.0 \mu\text{m}$, or $40.0 \mu\text{m}$, respectively). Force and PZA expansion were measured using the ZETOS load cell (Type 9011A, resolution 0.01 N, Kistler Instrument Corp., Amherst, NY) and PZA strain gages, respectively. These, in addition to time, were recorded for the calibration table generation.

2.3 Finite Element Analysis of Reference Bodies. FEA with ANSYS version 10.0 (ANSYS, Inc., Canonsburg, PA) was used to

simulate compression of the RBs in ZETOS. Axisymmetric models of each RB were meshed with an average of 6500 quadrilateral eight-noded elements and elastic modulus of 72.4 GPa [12]. Ideal geometries were used, including the threaded hole in the RB piston. After fabrication, the diaphragm thicknesses were verified with a CMM. These measurements demonstrated a percent error from ideal measurements of 0.545% and, thus, ideal dimensions were used to model the RBs instead of measured dimensions.

The FE models included all interface surfaces: the PZA crystal, the sapphire cylinder, the RB, and the loading platform (stainless steel base of 36 mm height). The interfaces were modeled with surface-to-surface contact elements (deformation of both surfaces), and the augmented Lagrangian contact algorithm. A maximum compressive displacement of $60.0 \mu\text{m}$ was defined on the top surface of the PZA crystal, which represents a $60.0 \mu\text{m}$ PZA expansion. The resultant reaction force (F) at the bottom of the RB was found. Displacement was obtained at the top of the RB piston and at the threaded cavity, subtracting from each the displacement at the bottom of the RB, to account for steel base deformation. RB rigidity was found for both displacement measurement sites using Eq. (1). The "true" rigidity, at the top of the RB piston, was required for the calibration table generation; the thread-derived rigidity was comparable to that measured in experiments, as described below.

2.4 Physical Testing of Reference Bodies. Six RBs were compressed in random order using a universal testing machine (Instron, Model 5566; 10 kN load cell, 0.5% accuracy), eight times each, at 0.06 mm/min. All the loading procedures were done at room temperature. A 10 mm diameter steel ball bearing (Fig. 4) was placed between the RB and compression platen to account for nonparallel surfaces and prevent moment transfer. Displacements were recorded as digital images using a microscope (Nikon Eclipse, Nikon Inc., Melville, NY) with a $10\times$ objective and a digital camera with resolution of 1280×1024 pixels (Model PL-A662, PixelINK, Ottawa, Canada). A preload of 10 ± 2 N was applied to the RB, at which point the device would automatically pause and hold for 30 s. During this pause, an image from the microscope was recorded. The loading continued until the final displacement. Again, the device would hold for another 30 s, when another image was recorded. The final input displacement was determined by trial and error, based on the real time reading from the fiber optic distance sensor, seeking a value of approximately $40 \mu\text{m}$. For each loading trial, two images of the rod tip were recorded: at the initial position (10 N preload) and at the end of the loading ramp. Adobe Illustrator, version 9.0.1 (Adobe Systems, Inc., San Jose, CA) was used to determine the net displacement by subtracting the rod's vertical coordinates at initial and final positions (resolution of $0.6 \mu\text{m}$, which is the length of one pixel, based on a calibration bar of $100 \mu\text{m}$).

The RBs were tested on a steel base to mimic the ZETOS loading platform. This was placed on the aluminum fixture, allowing the microscope's optimum measuring distance (Fig. 4) from the rod tip. Additional testing was done to determine the aluminum fixture rigidity. This was performed by placing a hollow cylinder on the fixture plus steel base arrangement. The hollow cylinder had similar dimensions to the RB and was used as a surrogate for the RB to contact and transfer load between the cross head and the steel base. The steel rod was placed through the hollow cylinder and through a 6 mm diameter hole on the steel base; with the support of a rubber ring, the upper rod tip was positioned just above the top surface of the steel base. This allowed the movement of the rod to represent the deformation of the fixture plus steel base arrangement. The lower rod-tip displacement was measured with the fiber optic distance sensor. The compliance (inverse of rigidity) of the fixture plus steel base arrangement was subtracted from the total compliance measured during testing of the RBs to determine the rigidity of the RBs.

2.5 Calibration Table Generation and Verification. The RB

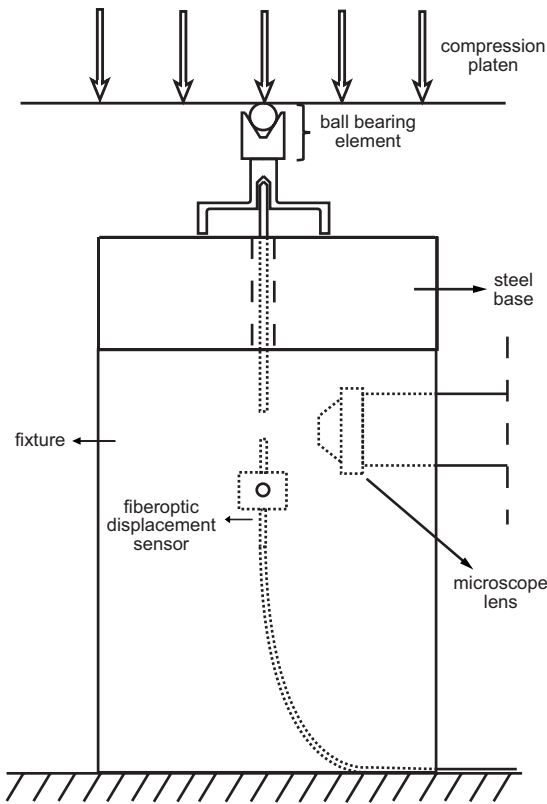


Fig. 4 Diagram (side view) of experimental setup used in the universal testing machine. The fixture has a c-shaped geometry (when viewed from the top) with the concavity on the front, allowing the microscope lens to be located near the rod tip for recording of digital images. Note also that the RB rests on a steel base, a solid block with a hole for the rod, to mimic the ZETOS system. This base is also included in the FEA. The diagram also shows the ball bearing element between the RB and the compression platen.

rigidity determined from physical testing using the universal testing machine was used to validate the FEA results. RB rigidity determined from experiments was compared with FEA-determined rigidity with a percent difference as follows:

$$\text{percent difference (\%)} = \frac{K_{\text{FEA}} - K_{\text{physical}}}{K_{\text{physical}}} \times 100 \quad (3)$$

The RB rigidity determined with FEA was used to generate the calibration table to relate force, PZA expansion, and RB deformation using spline interpolation. To verify the calibration table, the ten RBs were retested with the newly generated calibration table in ZETOS (following the protocol described in Sec. 2.4). The rigidity was taken as the slope of the last 50% of the force-displacement curve, using a linear fit. Percent differences of RB rigidity determined using ZETOS with respect to FE results were calculated as follows:

$$\text{percent difference (\%)} = \frac{K_{\text{ZETOS}} - K_{\text{FEA}}}{K_{\text{FEA}}} \times 100 \quad (4)$$

Three aluminum, custom-made springs (Fig. 5), each with a different rigidity, were tested in ZETOS and modeled with FEA. Both the experiment and the FE model included two sapphire cylinders, above and below the spring. Results were compared to FEA using Eq. (4). All the verification tests in ZETOS were performed at room temperature.

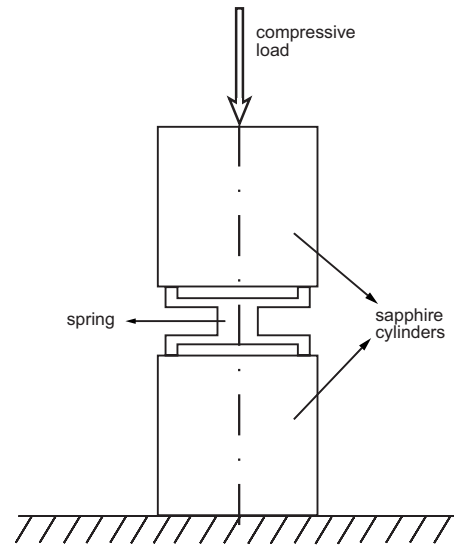


Fig. 5 Schematic showing the cross section of a cylindrical metallic spring specimen between two sapphire cylinders

3 Results

3.1 Reference Body Design. Two groups of RB geometries satisfied all design constraints (Fig. 2). The first group included six RBs and had a lateral wall thickness of 2 mm and fillet radii of 0.7 mm. The second group was comprised of four RBs, and had a lateral wall thickness of 4 mm and fillet radii of 1 mm. Diaphragm thickness varied in both geometries, 800.0–1800 μm for Geometry 1 and 1600–2200 μm for Geometry 2, obtaining a total rigidity range of 0.915–29.2 $\text{N}/\mu\text{m}$ or apparent elastic modulus of 58.3 MPa–1.86 GPa.

3.2 Finite Element Analysis of Reference Bodies. Table 1 shows the FE-determined rigidity for each RB based on deformation both at the top of the piston and in the thread. All RBs demonstrated a constant rigidity with respect to applied displacement (15.0–60.0 μm); that is, $R^2=1.00$ for each RB's force-displacement curve.

3.3 Physical Testing of the Reference Bodies. The RB rigidity was determined from each trial of physical compression testing using Eq. (1), where δ was the displacement calculated from the microscope images (Table 1). Simultaneous measurement with the fiber optic sensor allowed real time visualization of the force-displacement curve, revealing linear behavior (mean $R^2=1.00$). The percent difference, Eq. (3), of FEA-determined rigidity with respect to experimental results ranged from -4.22% to 5.80% .

3.4 Calibration Table Generation and Verification. A surface plot of the calibration table is presented in Fig. 6. The mean rigidity and standard deviation for each RB are shown in Table 2. The percent difference with respect to FEA-determined rigidity ranged from -2.84% to 2.52% . The rigidity measurements of the springs tested in ZETOS were 1.19 $\text{N}/\mu\text{m}$, 1.49 $\text{N}/\mu\text{m}$, and 1.68 $\text{N}/\mu\text{m}$, with percent differences with respect to FEA ranging from -4.55% to 0.658% .

4 Discussion

FEA was an effective tool for RB design. Geometric constraints were combined with material limitations to achieve a rigidity range representative of standard bone specimens. Two basic geometries were determined. Six RBs (the most compliant) belonged to Geometry 1, diaphragm thickness varying from 800 μm to 1800 μm ; four RBs belonged to Geometry 2, dia-

Table 1 Mean RB rigidity calculated with FEA and mean RB rigidity and standard deviation determined from physical testing on the universal testing machine (Sec. 2.4)

Reference body	FEA rigidity at piston (N/ μ m)	FEA rigidity at thread (N/ μ m)	Mean tested rigidity (SD) (N/ μ m)	Percent difference, FE (thread) versus physical testing (%)
1	0.915	0.914	0.864 (0.0104)	5.80
2	1.94	1.93	2.02 (0.0206)	-4.22
3	3.36	3.36		
4	5.13	5.15	5.07 (0.0538)	1.62
5	8.30	8.40		
6	11.9	12.2	11.9 (0.0577)	2.40
7	16.6	17.2	16.8 (0.287)	2.42
8	20.7	21.8		
9	24.9	26.7		
10	29.2	31.9	33.0 (0.480)	-3.20

Absolute mean percent difference (min., max) (%): 3.28 (-4.22,5.80)

phragm thickness ranging from 1600 μ m to 2200 μ m. In terms of rigidity, diaphragm thickness was the geometry's most important feature. According to plate theory, diaphragm deflection is directly related to thickness cubed, for plates with small thickness-to-radius ratio [11]. Although the most rigid RBs did not meet this criterion, the analytical relationship served as a useful starting point for the RB design.

The RBs were metallic to avoid nonlinearity and viscoelastic effects. Additionally, they were loaded within the elastic zone, avoiding permanent deformation. The rigidity range, 0.915–29.2 N/ μ m, was well distributed among the ten RBs, representing an apparent elastic modulus range of 58.3 MPa–1.86 GPa for standard bone specimens.

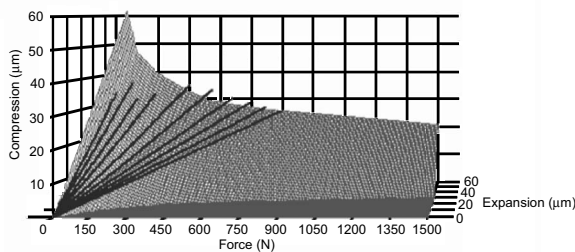


Fig. 6 Interpolated surface based on ZETOS force, expansion, and FEA compression of ten RBs

The axisymmetric FE model of RB compression in ZETOS provided valuable insight into the compliance of individual components. Both sapphire cylinders and PZA crystal underwent deformation, especially with the most rigid RBs. A displacement of 60.0 μ m (representing PZA expansion) at the top of the PZA crystal resulted in a RB compressive deformation of just 52.0 μ m for RB10. This demonstrates how PZA expansion differs from specimen deformation, thus the need of a calibration table. The steel base also experienced small deformation, with a maximum of 0.364 μ m (RB10). The ability of the FEA to isolate RB deformation allowed an accurate calculation of rigidity without compliance effects.

Care was taken to account for nonparallel surfaces during physical testing with a ball bearing element between the RB and compression platen. The 10 N preload was sufficient for settling contacting surfaces, resulting in a linear force-displacement curve. The noncontacting microscope measuring method for displacement calculation was appropriate although small errors may have resulted from resolution or image processing issues. Also, the sensitivity of both the load cell and microscope measurements could have induced additional error. Results from this experiment were similar to those from FEA, with a percent difference of -4.22–5.80%, serving as FEA validation. Because of the ability to completely isolate compliance of the RB, FEA results were used for the calibration table generation.

ZETOS testing of RBs with the calibration table resulted in differences between -2.84% and 2.52% with respect to FEA results. There was a low variance in the rigidity, with standard deviation

Table 2 Mean rigidity and standard deviation measured in the ZETOS system with the calibration table, and comparison with rigidity calculated using FEA

Reference body	ZETOS rigidity (SD) (N/ μ m)	FEA rigidity at piston (N/ μ m)	Percent difference, ZETOS versus FEA (%)
1	0.889 (0.0114)	0.915	-2.84
2	1.94 (0.00916)	1.94	0.00
3	3.38 (0.0220)	3.36	0.595
4	5.13 (0.0717)	5.13	0.00
5	8.36 (0.101)	8.30	0.723
6	12.2 (0.074)	11.9	2.52
7	16.6 (0.138)	16.6	0.00
8	20.4 (0.313)	20.7	-1.45
9	24.4 (0.271)	24.9	-2.01
10	28.9 (0.324)	29.2	-1.03

Absolute mean percent difference (min, max) (%): 1.12 (-2.84,2.52)

viations ranging from 0.00916 N/ μ m to 0.324 N/ μ m [coefficient of variation (COV) 0.472–1.12%]. Testing of the custom-made springs also demonstrated low variance and served as further validation of the recalibration procedure. Their FEA-determined rigidities were relatively low, 1.19–1.76 N/ μ m, representative of low-modulus cancellous bone cores (75.8–112.0 MPa). These values were corroborated with ZETOS, obtaining percent differences, with respect to FEA, ranging from –4.55% to 0.658%. Not only did ZETOS correctly measure the rigidity, but due to its low variance (standard deviation from 0.00378 N/ μ m, COV 0.318%, to 0.0298 N/ μ m, COV of 1.77%), it also had the capability of discerning between close values: the minimum rigidity difference was 0.19 N/ μ m (calculated from FEA).

5 Conclusion

A practical and successful calibration procedure for the ZETOS bone loading system has been presented. Calibration and testing results, including those from compression tests of custom-made springs, demonstrated that the ZETOS loading system was well calibrated, satisfactorily comparing to FEA, with a percent difference range of –4.55% to 0.658%. RBs and validated FEA offer a simple alternative for periodic evaluation and recalibration without the need of special testing equipment. The RBs are durable and may be used for regular calibration and with other testing systems. An accurate loading system is required for investigations of human bone mechanotransduction in a controlled environment to evaluate osteoporosis interventions and treatments, among other applications. The recalibration procedure is relevant for other ZETOS users and may also be applied to other testing systems for small specimens of compliant materials.

Acknowledgment

The authors are grateful to the main developers of the ZETOS system. Also, Professor Greg Nellis, Professor Scott Sanders, Pro-

fessor Donald Stone, and Professor Wendy Crone, University of Wisconsin–Madison, for their assistance with their knowledge and equipment; Adam Creuziger, Ph.D. candidate, University of Wisconsin–Madison for his help in the physical testing stage of the project; the University of Wisconsin–Madison Graduate School, and Eckhard Broeckmann.

References

- [1] Riggs, B. L., and Melton, L. J., 1995, “The Worldwide Problem of Osteoporosis: Insights Afforded by Epidemiology,” *Bone* (N.Y.), **17**(5), pp. 505S–511S.
- [2] Vanness, D. J., and Tosteson, N. A., 2005, “Estimating Opportunity Costs of Osteoporosis in the United States,” *Topics in Geriatric Rehabilitation*, **21**(1), pp. 4–16.
- [3] Jones, D. B., Broeckmann, E., Pohl, T., and Smith, E. L., 2003, “Development of a Mechanical Testing and Loading System for Trabecular Bone Studies for Long Term Culture,” *Eur. Cells Mater*, **5**, pp. 48–60.
- [4] Smith, E. L., Martens, F., Koller, K., Clark, W., and Jones, D. B., 2000, “The Effects of 20 Days of Mechanical Loading Plus PTH on the E-Modulus of Cow Trabecular Bone,” *American Society for Bone and Mineral Research (ASBMR) 22nd Annual Meeting*, Toronto, Canada, Vol. 15, p. s247.
- [5] Smith, E. L., Boudriot, U., Daume, B., Kratz, M., Jones, D. B., and Cullen, D. M., 2001, “Long Term Perfusion Loading of Trabecular Bone Cores and Formation Rate,” *American Society for Bone and Mineral Research (ASBMR) 22nd Annual Meeting*, Seattle, Washington, Vol. 16, p. s481.
- [6] Davies, C. M., Jones, D. B., Stoddart, M. J., Koller, K., Smith, E., Archer, C. W., and Richards, R. G., 2006, “Mechanically Loaded *Ex Vivo* Bone Culture System ‘Zetos’: Systems and Culture Preparation,” *Eur. Cells Mater*, **11**, pp. 57–75.
- [7] Currey, J., 1984, *The Mechanical Adaptations of Bones*, Princeton University Press, Princeton, NJ, pp. 133–137.
- [8] Martin, R. B., Burr, D. B., and Sharkey, N. A., 1998, *Skeletal Tissue Mechanics*, Springer, New York, pp. 127–180.
- [9] Cowin, S. C., 2001, *Bone Mechanics Handbook*, CRC, Boca Raton, FL, pp. 15.1–15.24.
- [10] Rohl, L., Larsen, E., Linde, F., Odgaard, A., and Jorgensen, J., 1991, “Tensile and Compressive Properties of Cancellous Bone,” *J. Biomech.*, **24**(12), pp. 1143–1149.
- [11] Timoshenko, S., 1940, *Theory of Plates and Shells*, McGraw-Hill, New York, pp. 51–78.
- [12] 1990, *Metals Handbook: Properties and Selection: Nonferrous Alloys and Special-Purpose Materials*, 10th ed., ASM International, Metals Park, OH, Vol. 2.